Way Points and Reference Speed Based Trajectory Generator for an Unmanned Surface Vehicle

Hongkun He[1(✉)] and Ning Wang[2]

[1] School of Marine Electrical Engineering, Dalian Maritime University, Dalian 116026, China
hehongkun4@163.com

[2] School of Marine Engineering, Dalian Maritime University, Dalian 116026, China
n.wang@ieee.org

Abstract. On the basis of successive way points (WPs) and piecewise reference speed, a trajectory generator (TG) is elaborately devised to generate a smooth trajectory for an unmanned surface vehicle (USV) in this paper. Firstly, the seventh-order polynominal is exclusively deployed to fit foregoing WPs, resulting in the parameterized path with sufficient differentiability. Then, the reference speed passes through the second-order filter, such that the speed command is uniformly continuous. Together with the parameterized path and speed command, the path speed is readily designed, and thereby contributing to the continuously differentiable trajectory. Certainly, the desired trajectory is much easier for users to predesignate in the electronic chart, and is more favorable to be exactly tracked by the USV in practice. Eventually, the model-based controller for the USV is synthesized to asymptotically track the generated trajectory in the absence of unmodeled dynamics and external disturbances. Comprehensive simulations are conducted on the benchmark prototype CyberShip II, so as to validate the effectiveness of both the proposed TG and trajectory-tracking controller.

Keywords: Unmanned surface vehicle (USV) · Trajectory generator (TG) · Way points (WPs) · Seventh-order polynominal · Second-order filter

1 Introduction

As an ocean robot, the unmanned surface vehicle (USV) can replace humans to execute dangerous and repetitive tasks, and thereby playing an increasingly important role in the marine community [3,16–18]. In some cases, the USV should reach the desired position with the prescribed time and course angle, e.g.,

This work is supported by the National Natural Science Foundation of China (Grant 52271306) and Innovative Research Foundation of Ship General Performance (Grant 31422120).

H. R. Karimi and N. Wang (Eds.): S-Cube 2022, LNICST 487, pp. 3–16, 2023.
https://doi.org/10.1007/978-3-031-34899-0_1

the hydrographic survey of restricted access areas [11]. Therefore, the trajectory tracking control of the USV involving both spatial and temporal constraints, has great application potential in engineering [5,15,22]. Naturally, the trajectory-tracking problem has also attracted extensive attention from researchers, investigating challenges and sharing latest results from different perspectives [14,23,25].

Note that, the USV moves on the water to track the desired trajectory, and would suffer from complex uncertainties arising from itself and surrounding environments, including unmodeled dynamics and external disturbances[13]. With respect to the parameter perturbation problem, a new guidance law has been constructed for an underactuated USV in [4], wherein nonlinear tracking differentiators are introduced to obtain derivative signals instead of the first-order filter, achieving satisfactory differential performance and fast trajectory-tracking response. In addition to internal uncertainties of the USV, external disturbances have been exactly observed by the disturbance estimator [8], and the resultant controller is derived from the backstepping technique, rendering trajector-tracking errors globally exponentially stable. To further enhance the ability of disturbance rejection, the finite-time control scheme has been created in [19], whereby the finite-time disturbance observer and nonsingular fast terminal sliding-mode manifold are combined, such that both disturbance observation and trajectory-tracking errors can be finite-time stable. Since the settling time of the finite-time control method is related to initial states, a novel fixed-time nonsingular sliding mode manifold [24] has been developed according to the bi-limit homogeneous theory, and thereby resulting in the fixed-time trajectory-tracking scheme for the USV, making both position and velocity errors converge to the origin within a fixed settling time, certainly in the presence of model uncertainties and external disturbances.

Besides the disturbance rejection, other prominent problems behind the trajectory tracking control of the USV have been also widely researched in the existing literature. In [6], both error constraints and input saturation have been taken into account, thereby the tan-type barrier Lyapunov function is used to remain trajectory-tracking errors within the prescribed regions, and the hyperbolic tangent function to deal with the saturation problem. Since the control execution is often periodic, the computational cost is rather expensive. Aiming at both faster convergence rate and lower computational burden, a novel event-triggered adaptive practical fixed-time fuzzy controller has been proposed in [10]. When working for a long time at sea, the USV may suffer from the actuator fault problem. In [7], an adaptive neural network-based fault-tolerant trajectory-tracking controller has been proposed in combination with the parameter adaptive method and the radial basis function neural networks. Furthermore, the actuator dead-zone problem has been elegantly solved by a finite-time trajectory-tracking control method [2], wherein time-varying input coefficients are also regarded as system uncertainties, and are exactly observed by a robust homogeneous differentiator.

Although a lots of challenges have been skillfully overcome by aforementioned works, a practically fundamental problem has not been sufficiently touched, i.e., how to generate a feasibly desired trajectory. In [10], the reference trajectory

and its derivatives have been assumed to be available, but how to obtain it is not mentioned. In [4,6–8,24,25], sine and cosine functions have been used to directly predefine the sinusoidal, circular or straight trajectories. Since the trigonometric function is sufficiently differentiable, the resultant trajectory is absolutely continuous [21]. Clearly, the reference signal can be smoothly tracked by the USV, and thereby resulting in a simple trajectory-generation method. Moreover, another prevailing method is adopting a virtual ship to generate the desired trajectory [2,5,12,19,20,22]. In fact, the trajectory is driven by the nominal model of the USV, whereby unmodeled dynamics and external disturbances are reasonably neglected. Since the desired and actual systems are in the same form, the resultant trajectory is feasible to be tracked by the USV. It should be highlighted that, it is rather difficult to determine setup parameters of both trigonometric function and virtual ship methods, such that the configuration of generated trajectory can be arbitrarily changed according to human intentions. In this context, foregoing methods are infeasible in practice.

To solve the trajectory-generation problem from a practical viewpoint, a trajectory generator (TG) is devised on the basis of successive way points (WPs) and reference speed in this paper. Actually, it is not hard for users to predesignate these WPs in the electronic chart. Furthermore, the reference speed can be allowed to be piecewisely constant, such that it is easy for users to assign values. To guarantee sufficient differentiability, a seventh-order polynominal is exclusively deployed to fit WPs in sequence, and thereby resulting in a parameterized path. To smooth the reference speed, a second-order filter is employed, making the speed command uniformly continuous. In combination with the parameterized path and speed command, the desired trajectory is readily generated by designing the path speed. Based on the model information, a PD-like controller is also synthesized for the USV to track the generated trajectory, and the closed-loop system is strictly proven to be asymptotically stable. Comprehensive simulations are conducted on the CyberShip II, so as to validate the effectiveness of both the proposed TG and trajectory-tracking controller.

The remainder of this paper is arranged as follows. Section 2 formulates the concerned problem. The proposed TG and trajectory-tracking controller is presented in Sect. 3. Simulation results are given in Sect. 4. This paper is concluded in Sect. 5.

2 Problem Formulation

The USV is assumed to move in a calm water when tracking a desired trajectory, and thus magnitudes of pith, roll and heave motions are quiet small, such that they can be reasonably neglected. To facilitate the problem formulation, as shown in Fig. 1, the earth-fixed coordinate frame EXY is built with X and Y axes pointing towards the north and east, respectively. In addition, the frame BX_bY_b is fixed to the USV, wherein the point B is the geometric center, X_b and Y_b axes are directing to the fore and starboard, respectively. In this context, the USV can be modeled in EXY and BX_bY_b for kinematics and dynamics, respectively,

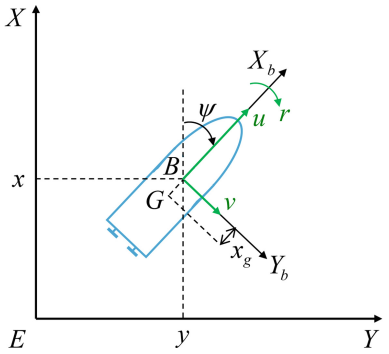

Fig. 1. Earth- and body-fixed coordinate frames of the USV.

which is presented as follows [1]

$$\dot{\boldsymbol{\eta}} = \boldsymbol{R}(\psi)\boldsymbol{\nu} \tag{1a}$$

$$\boldsymbol{M}\dot{\boldsymbol{\nu}} = -\boldsymbol{C}(\boldsymbol{\nu})\boldsymbol{\nu} - \boldsymbol{D}(\boldsymbol{\nu})\boldsymbol{\nu} + \boldsymbol{\tau} \tag{1b}$$

where $\boldsymbol{\eta} = [x, y, \psi]^T$ is the pose vector consisting of position coordinates (x, y) and yaw angle $\psi \in (-\pi, \pi]$ in EXY, $\boldsymbol{\nu} = [u, v, r]^T$ denotes the velocity vector including surge/sway velocities (u, v) and angular rate r in BX_bY_b, and $\boldsymbol{\tau} = [\tau_u, \tau_v, \tau_r]^T$ represents the control input vector.

Moreover, $\boldsymbol{R}(\psi)$ denotes the rotation matrix from EXY to BX_bY_b, $\boldsymbol{M}$ represents the inertia matrix including hydrodynamic added masses, $\boldsymbol{C}(\boldsymbol{\nu})$ and $\boldsymbol{D}(\boldsymbol{\nu})$ are Coriolis/centripetal and damping matrices, respectively. For readability, aforementioned matrices are intensively given by

$$\boldsymbol{M} = \begin{bmatrix} m_{11} & 0 & 0 \\ 0 & m_{22} & m_{23} \\ 0 & m_{32} & m_{33} \end{bmatrix} \tag{2a}$$

$$\boldsymbol{R}(\psi) = \begin{bmatrix} \cos\psi & -\sin\psi & 0 \\ -\sin\psi & \cos\psi & 0 \\ 0 & 0 & 1 \end{bmatrix} \tag{2b}$$

$$\boldsymbol{D}(\boldsymbol{\nu}) = \begin{bmatrix} d_{11}(\boldsymbol{\nu}) & 0 & 0 \\ 0 & d_{22}(\boldsymbol{\nu}) & d_{23}(\boldsymbol{\nu}) \\ 0 & d_{32}(\boldsymbol{\nu}) & d_{33}(\boldsymbol{\nu}) \end{bmatrix} \tag{2c}$$

$$\boldsymbol{C}(\boldsymbol{\nu}) = \begin{bmatrix} 0 & 0 & -m_{11}v - m_{23}r \\ 0 & 0 & -m_{11}u \\ m_{11}v + m_{23}r & m_{11}u & 0 \end{bmatrix} \tag{2d}$$

where $m_{11} = m - X_{\dot{u}}$, $m_{22} = m - Y_{\dot{v}}$, $m_{23} = mx_g Y_{\dot{r}}$, $m_{32} = mx_g - N_{\dot{v}}$, $m_{33} = I_z - N_{\dot{r}}$, $d_{11}(\boldsymbol{\nu}) = -X_u - X_{|u|u}|u| - X_{uuu}u^2$, $d_{22}(\boldsymbol{\nu}) = -Y_v - Y_{|v|v}|v| - Y_{|r|v}|r|$, $d_{23}(\boldsymbol{\nu}) = -Y_r - Y_{|v|r}|v| - Y_{|r|r}|r|$, $d_{32}(\boldsymbol{\nu}) = -N_v - N_{|v|v}|v| - N_{|r|v}|r|$, and $d_{33}(\boldsymbol{\nu}) = -N_r - N_{|v|r}|v| - N_{|r|r}|r|$. Here, m is the mass of the USV, I_z is the movement inertia about yaw motions, and x_g is the distance between B

and the gravity center G as shown in Fig. 1. Besides, all terms X_*, Y_* and N_* consistently represent hydrodynamic derivatives.

In engineering, the USV is deployed to explore some waters by simply tracking the desired trajectory $\boldsymbol{\eta}_d = [x_d, y_d, \psi_d]^T$. In the existing literature, the trigonometric function method [4,6–8,24,25] predefines the time-varying signal as follows

$$\boldsymbol{\eta}_d(t) = \boldsymbol{f}(\cos(t), \sin(t), t) \tag{3}$$

where $\boldsymbol{f}(\cdot)$ is sufficiently differentiable. Derived from (1), the virtual ship method [2,5,12,19,20,22] is formulated by

$$\dot{\boldsymbol{\eta}}_d = \boldsymbol{R}(\psi_d)\boldsymbol{\nu}_d \tag{4a}$$

$$\boldsymbol{M}\dot{\boldsymbol{\nu}}_d = -\boldsymbol{C}(\boldsymbol{\nu}_d)\boldsymbol{\nu}_d - \boldsymbol{D}(\boldsymbol{\nu}_d)\boldsymbol{\nu}_d + \boldsymbol{\tau}_d \tag{4b}$$

where $\boldsymbol{\tau}_d$ is the desired input vector, $\boldsymbol{\eta}_d$ and $\boldsymbol{\nu}_d$ are desired outputs.

Clearly, both trigonometric function and virtual ship methods are rather abstract, since it is difficult to intuitively determine setup parameters of (3) and (4), such that the resultant trajectory can be arbitrarily changed, so as to satisfy practical requirements. In this context, it seems like a big barrier between the theory and practice for trajectory tracking of the USV. From a practical viewpoint, it is pretty easier for practitioners to plan the trajectory-tracking task in the electronic chart by prescribing a sequence of WPs as follows

$$\boldsymbol{p}_{d_i} = [x_{d_i}, y_{d_i}]^T \tag{5}$$

where $i = 1, 2, \cdots, n$, and n is the number of WPs. Therefore, how to generate a feasibly desired trajectory based on prescribed WPs (5) are exclusively taken into account in this paper.

To clearly demarcate the edge of our concerned problem, a assumption is reasonably made as follows.

Assumption 1. *All model parameters in (1) have been previously identified to facilitate controller designs, in addition that unmodeled dynamics and external disturbances are sufficiently small such that they can be reasonably neglected.*

Instead of both the trigonometric function method (3) and virtual ship approach (4), the main objective of this paper is to invent a generalized method that can generate a smooth trajectory passing through successive WPs (5) with programmable course and velocities. Besides, another objective is to design the control input $\boldsymbol{\tau}$ in (1) such that the generated trajectory can be tracked by the USV.

3 Trajectory Generation and Control Design

3.1 Trajectory Generation

As shown in Fig. 2, a series of WPs are predesignated by users in the electronic chart. Certainly, it is not easy to generate a trajectory passing these WPs by

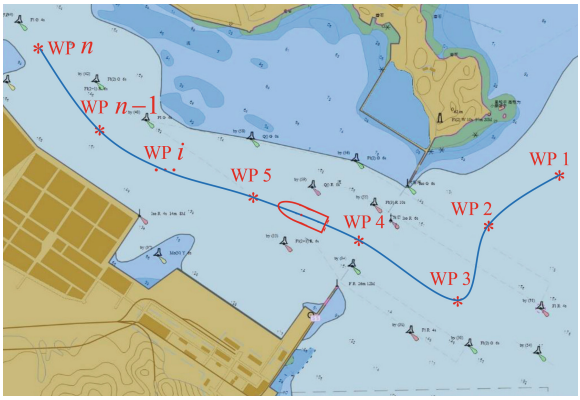

Fig. 2. The USV is maneuvering from WP to WP along a smooth trajectory.

virtue of the trigonometric function (3) or virtual ship (4). In the proposed TG, a parameterized path is firstly planned on the basis of spacial constraints, then it is transformed into the desired trajectory by applying temporal constraints. In contrast, our method is more intuitive and practical in engineering.

To be specific, an unique parameterized value θ_i is attached to each WP in (5), i.e.,

$$\boldsymbol{p}_d(\theta_i) = [x_d(\theta_i), y_d(\theta_i)]^T. \tag{6}$$

Without loss of generality, θ_i is simply determined by

$$\theta_i = i - 1. \tag{7}$$

In other words, these successive WPs are starting at WP 1 with $\theta_1 = 0$ and are ending at WP n with $\theta_n = n - 1$.

In the sequel, a seventh-order polynomial is employed to interpolate foregoing data, and thereby the parameterized subpath from WP i to WP $i + 1$ can be mathematically formulated by

$$\boldsymbol{p}_d(\theta) = \boldsymbol{B}\boldsymbol{\theta}_7 \tag{8}$$

with

$$\boldsymbol{B} = \begin{bmatrix} b_{x_7}, b_{x_6}, \cdots, b_{x_1}, b_{x_0} \\ b_{y_7}, b_{y_6}, \cdots, b_{y_1}, b_{y_0} \end{bmatrix} \tag{9a}$$

$$\boldsymbol{\theta}_7 = [(\theta - \theta_i)^7, (\theta - \theta_i)^6, \cdots, (\theta - \theta_i), 1]^T \tag{9b}$$

where θ is the parameterized variable.

Note that the coefficient matrix $\boldsymbol{B}$ in (8) is inherently unknown, and it needs sixteen constraint equations at least to solve these coefficients. To guarantee both the continuity and differentiability of $\boldsymbol{p}_d(\theta)$ at WP i, spacial constraints

are required as follows

$$\boldsymbol{p}_d(\theta_i) = \boldsymbol{p}_{d_i} \tag{10a}$$

$$\left.\frac{\partial \boldsymbol{p}_d(\theta)}{\partial \theta}\right|_{\theta=\theta_i} = \begin{cases} \boldsymbol{p}_d(\theta_{i+1}) - \boldsymbol{p}_d(\theta_i) & i = 1 \\ k\left(\boldsymbol{p}_d(\theta_{i+1}) - \boldsymbol{p}_d(\theta_i)\right) & i \in (1, n) \\ \boldsymbol{p}_d(\theta_i) - \boldsymbol{p}_d(\theta_{i-1}) & i = n \end{cases} \tag{10b}$$

$$\left.\frac{\partial^2 \boldsymbol{p}_d(\theta)}{\partial \theta^2}\right|_{\theta=\theta_i} = \begin{cases} \left.\frac{\partial \boldsymbol{p}_d(\theta)}{\partial \theta}\right|_{\theta=\theta_{i+1}} - \left.\frac{\partial \boldsymbol{p}_d(\theta)}{\partial \theta}\right|_{\theta=\theta_i} & i = 1 \\ k\left(\left.\frac{\partial \boldsymbol{p}_d(\theta)}{\partial \theta}\right|_{\theta=\theta_{i+1}} - \left.\frac{\partial \boldsymbol{p}_d(\theta)}{\partial \theta}\right|_{\theta=\theta_i}\right) & i \in (1, n) \\ \left.\frac{\partial \boldsymbol{p}_d(\theta)}{\partial \theta}\right|_{\theta=\theta_i} - \left.\frac{\partial \boldsymbol{p}_d(\theta)}{\partial \theta}\right|_{\theta=\theta_{i-1}} & i = n \end{cases} \tag{10c}$$

$$\left.\frac{\partial^3 \boldsymbol{p}_d(\theta)}{\partial \theta^3}\right|_{\theta=\theta_i} = \begin{cases} \left.\frac{\partial^2 \boldsymbol{p}_d(\theta)}{\partial \theta^2}\right|_{\theta=\theta_{i+1}} - \left.\frac{\partial^2 \boldsymbol{p}_d(\theta)}{\partial \theta^2}\right|_{\theta=\theta_i} & i = 1 \\ k\left(\left.\frac{\partial^2 \boldsymbol{p}_d(\theta)}{\partial \theta^2}\right|_{\theta=\theta_{i+1}} - \left.\frac{\partial^2 \boldsymbol{p}_d(\theta)}{\partial \theta^2}\right|_{\theta=\theta_i}\right) & i \in (1, n) \\ \left.\frac{\partial^2 \boldsymbol{p}_d(\theta)}{\partial \theta^2}\right|_{\theta=\theta_i} - \left.\frac{\partial^2 \boldsymbol{p}_d(\theta)}{\partial \theta^2}\right|_{\theta=\theta_{i-1}} & i = n \end{cases} \tag{10d}$$

where $k > 0$ is used to design the curvature at WP i, and thereby $\boldsymbol{B}$ can be determined by (10).

In essence, the desired position of the USV is predefined by the path (8), and thereby the desired course angle can be naturally determined by its tangent angle, i.e.,

$$\psi_d(\theta) = \text{atan2}(\frac{\partial y_d(\theta)}{\partial \theta}, \frac{\partial x_d(\theta)}{\partial \theta}) \tag{11}$$

where atan2$(\cdot)$ is the four-quadrant arc-tangent function. Therefore, the desired configuration of the USV can be given by

$$\boldsymbol{\eta}_d(\theta) = [\boldsymbol{p}_d^T(\theta), \psi_d(\theta)]^T. \tag{12}$$

In addition, users should also prespecify the reference speed $u_r > 0$ as the temporal constraints to generate the desired trajectory. Certainly, it is easier for users to assign piecewise constant values to u_r. However, such a reference signal is not sufficiently smooth and can not be tracked immediately by the USV. As a result, the second-order low-pass filter can be exploited as follows

$$\ddot{u}_d + 2\iota\varsigma\dot{u}_d + \varsigma^2 u_d = \varsigma^2 u_r \tag{13}$$

where $u_d \geq 0$ is the continuous speed command, $\iota > 0$ and $\varsigma > 0$ are the damping ratio and natural frequency of the filter, respectively.

Eventually, the desired trajectory $\boldsymbol{\eta}_d(t)$ can be obtained from (12) by designing the path speed

$$\dot{\theta} = \frac{u_d(t)}{\sqrt{\left(\frac{\partial y_d(\theta)}{\partial \theta}\right)^2 + \left(\frac{\partial x_d(\theta)}{\partial \theta}\right)^2}} \tag{14}$$

and the desired dynamics are given by

$$\dot{\boldsymbol{\eta}}_d = \frac{\partial \boldsymbol{\eta}_d}{\partial \theta}\dot{\theta} \tag{15a}$$

$$\ddot{\boldsymbol{\eta}}_d = \frac{\partial^2 \boldsymbol{\eta}_d}{\partial \theta^2}\dot{\theta}^2 + \frac{\partial \boldsymbol{\eta}_d}{\partial \theta}\left(\frac{\partial \dot{\theta}}{\partial \theta}\dot{\theta} + \frac{\partial \dot{\theta}}{\partial t}\right). \tag{15b}$$

Note that $\ddot{\boldsymbol{\eta}}_d$ is expected to be continuous, which implies that $\frac{\partial^3 \boldsymbol{p}_d(\theta)}{\partial \theta^3}$ should be continuous as shown in (11). That is why we choose the seventh-order polynomial at least to fit given WPs as demonstrated in (10d).

3.2 Control Design

From (1a), we redefine a new variable $\boldsymbol{\omega} = \boldsymbol{R}(\psi)\boldsymbol{\nu}$, which represents the USV velocity vector expressed in EXY. As usual, the trajectory-tracking and velocity-tracking errors are defined by $\boldsymbol{e}_\eta = \boldsymbol{\eta} - \boldsymbol{\eta}_d$ and $\boldsymbol{e}_\omega = \boldsymbol{\omega} - \dot{\boldsymbol{\eta}}_d$, respectively. Taking the time derivative of $\boldsymbol{e}_\eta$ along (1) and (15) yields

$$\dot{\boldsymbol{e}}_\eta = \boldsymbol{e}_\omega \tag{16a}$$

$$\dot{\boldsymbol{e}}_\omega = \boldsymbol{S}(\omega_\psi)\boldsymbol{\omega} - \boldsymbol{R}(\psi)\boldsymbol{M}^{-1}(\boldsymbol{C}(\boldsymbol{\nu})\boldsymbol{\nu} + \boldsymbol{D}(\boldsymbol{\nu})\boldsymbol{\nu} - \boldsymbol{\tau}) - \ddot{\boldsymbol{\eta}}_d \tag{16b}$$

where $\boldsymbol{e}_\eta := [e_{\eta_1}, e_{\eta_2}, e_{\eta_3}]^T$, $\boldsymbol{e}_\omega := [e_{\omega_1}, e_{\omega_2}, e_{\omega_3}]^T$, $\boldsymbol{\omega} := [\omega_x, \omega_y, \omega_\psi]^T$, and $\boldsymbol{S}(\omega_\psi) = \begin{bmatrix} 0 & -\omega_\psi & 0 \\ \omega_\psi & 0 & 0 \\ 0 & 0 & 0 \end{bmatrix}$.

Since the error system (16) possesses the canonical form of linear integral chain, the trajectory-tracking controller can be easily designed by

$$\boldsymbol{\tau} = \boldsymbol{C}(\boldsymbol{\nu})\boldsymbol{\nu} + \boldsymbol{D}(\boldsymbol{\nu}) + \boldsymbol{M}\boldsymbol{R}^T(\psi)(\ddot{\boldsymbol{\eta}}_d - \boldsymbol{S}(\omega_\psi)\boldsymbol{\omega} - \boldsymbol{K}_p\boldsymbol{e}_\eta - \boldsymbol{K}_d\boldsymbol{e}_\omega) \tag{17}$$

where $\boldsymbol{K}_p = \mathrm{diag}(k_{p1}, k_{p2}, k_{p3}) > 0$ and $\boldsymbol{K}_d = \mathrm{diag}(k_{d1}, k_{d2}, k_{d3}) > 0$.

Theorem 1. *Under the Assumption 1, the proposed controller (17) can make the trajectory-tracking system (16) asymptotically stable.*

Proof. Substituting (17) into (16) yields the closed-loop system

$$\dot{\boldsymbol{e}} = \boldsymbol{K}\boldsymbol{e} \tag{18}$$

where $\boldsymbol{e} = [\boldsymbol{e}_\eta^T, \boldsymbol{e}_\omega^T]^T$, and $\boldsymbol{K} = \begin{bmatrix} \boldsymbol{0}_{3\times 3} & \boldsymbol{I}_{3\times 3} \\ -\boldsymbol{K}_p & -\boldsymbol{K}_d \end{bmatrix}$.

Note that it can be readily verify that $\boldsymbol{K}$ is a Hurwitz matrix. As a consequence, there exists an unique positive definite matrix $\boldsymbol{P} \in \mathbb{R}^{3\times 3}$ for any positive definite matrix $\boldsymbol{Q} \in \mathbb{R}^{3\times 3}$, such that

$$\boldsymbol{K}^T\boldsymbol{P} + \boldsymbol{P}\boldsymbol{K} = -\boldsymbol{Q} \tag{19}$$

always holds.

Consider the Lyapunov candidate as follows

$$V = \boldsymbol{e}^T \boldsymbol{P} \boldsymbol{e} \tag{20}$$

and differentiating V along (18) and (19) yields

$$\begin{aligned} \dot{V} &= -\boldsymbol{e}^T \boldsymbol{Q} \boldsymbol{e} \\ &\leq -\frac{\lambda_{\min}(\boldsymbol{Q})}{\lambda_{\max}(\boldsymbol{P})} V \end{aligned} \tag{21}$$

where $\lambda_{\min}(\boldsymbol{Q}) > 0$ is the minimum eigenvalue of $\boldsymbol{Q}$, and $\lambda_{\max}(\boldsymbol{P}) > 0$ represents the maximum eigenvalue of $\boldsymbol{P}$.

From (21), we can immediately have $\dot{V} < 0$, which implies that V is asymptotically stable. Together with (20), we can eventually conclude that $\lim_{t\to\infty} \boldsymbol{e}_\eta(t) = \boldsymbol{0}_3$ and $\lim_{t\to\infty} \boldsymbol{e}_\omega(t) = \boldsymbol{0}_3$. This completes the proof.

4 Simulation Studies

To validate the effectiveness of both the proposed TG and trajectory-tracking controller in this section, the famous benchmark prototype CyberShip II [9] is deployed to conduct simulations, whereby its model parameters are intensively given in Table 1.

Table 1. Main model parameters of the CyberShip II [9].

Parameters	Values	Parameters	Values	Parameters	Values
m	23.8000	I_z	1.7600	x_g	0.0460
X_u	−0.7225	$X_{\dot{u}}$	−2.0000	Y_v	−0.8612
Y_r	0.1079	$Y_{\dot{v}}$	−10.0000	$Y_{\dot{r}}$	−0.0000
N_v	0.1052	N_r	−1.9000	$N_{\dot{v}}$	−0.0000
$N_{\dot{r}}$	−1.0000	$X_{\|u\|u}$	−1.3274	$Y_{\|v\|v}$	−36.2823
$Y_{\|v\|r}$	−0.8450	$Y_{\|r\|v}$	−8.0500	$Y_{\|r\|r}$	−3.4500
$N_{\|v\|v}$	5.0437	$N_{\|v\|r}$	0.0800	$N_{\|r\|v}$	0.1300
$N_{\|r\|r}$	−0.7500	X_{uuu}	−5.8664		

To setup simulations, a sequence of WPs are randomly predefined as shown in Table 2. In practice, they can be predesignated by users in light of the electronic chart, so as to generate the desired trajectory. To this end, the adjustable parameter is set by $k = 0.5$ to obtain a medium curvature, and the reference speed is simply selected as

$$u_r(t) = \begin{cases} 0.5 & t \in [0, 40] \\ 1 & t \in (40, 70] \\ 1.5 & t \in (70, 100] \\ 2 & t \in (100, 120] \end{cases}. \tag{22}$$

Table 2. A sequence of WPs used in simulations.

WPs	Values	WPs	Values	WPs	Values
$\boldsymbol{P}_{d_1}$	$[-28,-3]^T$	$\boldsymbol{P}_{d_2}$	$[-19,0]^T$	$\boldsymbol{P}_{d_3}$	$[-8,5]^T$
$\boldsymbol{P}_{d_4}$	$[0,-3]^T$	$\boldsymbol{P}_{d_5}$	$[6,0]^T$	$\boldsymbol{P}_{d_6}$	$[8,10]^T$
$\boldsymbol{P}_{d_7}$	$[5,30]^T$	$\boldsymbol{P}_{d_8}$	$[-10,33]^T$	$\boldsymbol{P}_{d_9}$	$[-20,30]^T$
$\boldsymbol{P}_{d_{10}}$	$[-28,25]^T$	$\boldsymbol{P}_{d_{11}}$	$[-28,15]^T$	$\boldsymbol{P}_{d_{12}}$	$[-20,5]^T$

In order to smooth this piecewise signal, the initial output of the second-order filter is chosen as $u_d(0) = 0$, its damping ratio and natural frequency $\iota = 0.5$ and $\varsigma = 0.5$, respectively.

4.1 Performance on the TG

Simulation results are shown in Fig. 3. By virtue of the proposed TG, as shown in Fig. 3(a), the generated trajectory passes through user-predesignated WPs in sequence, and corresponding tangent angle along the trajectory is set as the USV course angle. It should be highlighted that, as shown in Fig. 3(b), the trajectory is continuous in time, which is favorable for the USV to be tracked. Here, ψ_d is uniformly projected into $(-\pi, \pi]$ by the normalized operation. More importantly, as shown in Figs. 3(c) and 3(d), the desired velocity and acceleration are both continuous, which will not lead to switching control inputs when tracked by the USV. Actually, continuous signals $\boldsymbol{\eta}_d$, $\dot{\boldsymbol{\eta}}_d$ and $\ddot{\boldsymbol{\eta}}_d$ benefit from the seventh-order polynominal and second-order low-pass filter, which are exclusively incorporated into the proposed TG. Clearly, if we intend to generate the desired trajectory and its derivatives as same as Fig. 3, it is not easy to decide setup parameters when using the trigonometric function or virtual ship method. In this context, the proposed TG is more intuitive and practical.

4.2 Performance on the Trajectory-Tracking Controller

To track the generated trajectory by the USV, the PD-like trajectory-tracking controller is synthesized in this paper. In simulations, initial states of the USV are set as $\boldsymbol{\eta}(0) = [-30, 2, -0.4]^T$ and $\boldsymbol{\nu}(0) = [0, 0, 0]^T$. Furthermore, control gains are simply given by $\boldsymbol{K}_p = \mathrm{diag}(0.1, 0.1, 0.1)$ and $\boldsymbol{K}_d = \mathrm{diag}(0.5, 0.5, 0.5)$.

Simulation results are shown in Fig. 4. Thanks to the smooth trajectory generated by the proposed TG, all control inputs of the USV are continuous as shown in Fig. 4(a), although the reference velocity is piecewise. Clearly, continuous signals are easier to be implemented by practical actuators. In this sense, the

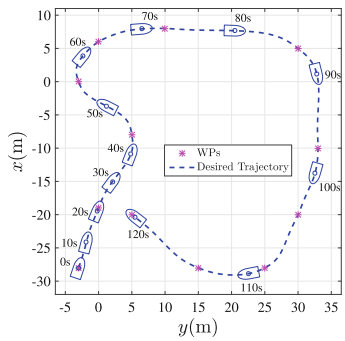

(a) The desired trajectory

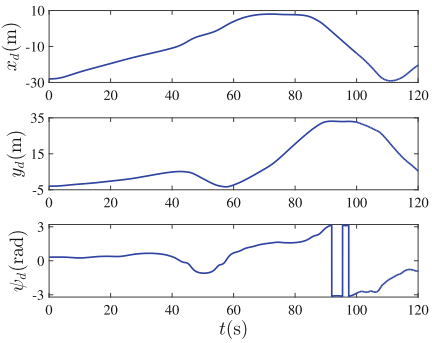

(b) The desired pose $\boldsymbol{\eta}_d$

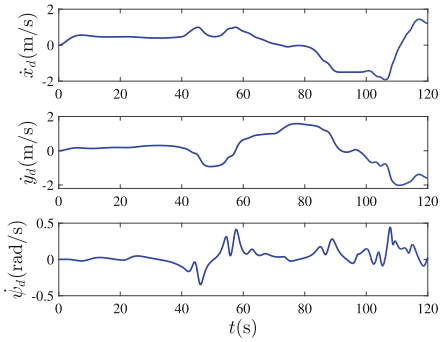

(c) The desired velocity $\dot{\boldsymbol{\eta}}_d$

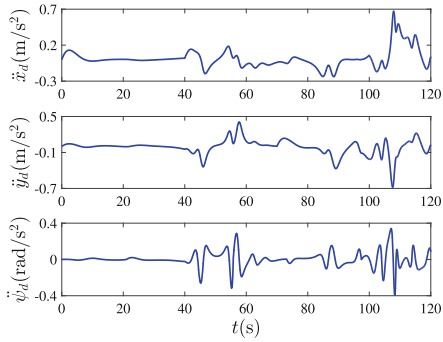

(d) The desired acceleration $\ddot{\boldsymbol{\eta}}_d$

Fig. 3. The reference signals generated by the proposed TG.

consideration of continuity and differentiability when devising the TG is vital for applications. Moreover, driven by the continuous controller, both trajectory- and velocity-tracking errors asymptotically converge to zero as shown in Figs. 4(b) and 4(c), respectively. Note that these results are consistent with the Theorem 1 and corresponding stability analyses. Eventually, as shown in Fig. 4(d), the desired trajectory is exactly tracked by the USV in the absence of unmodeled dynamics and external disturbances.

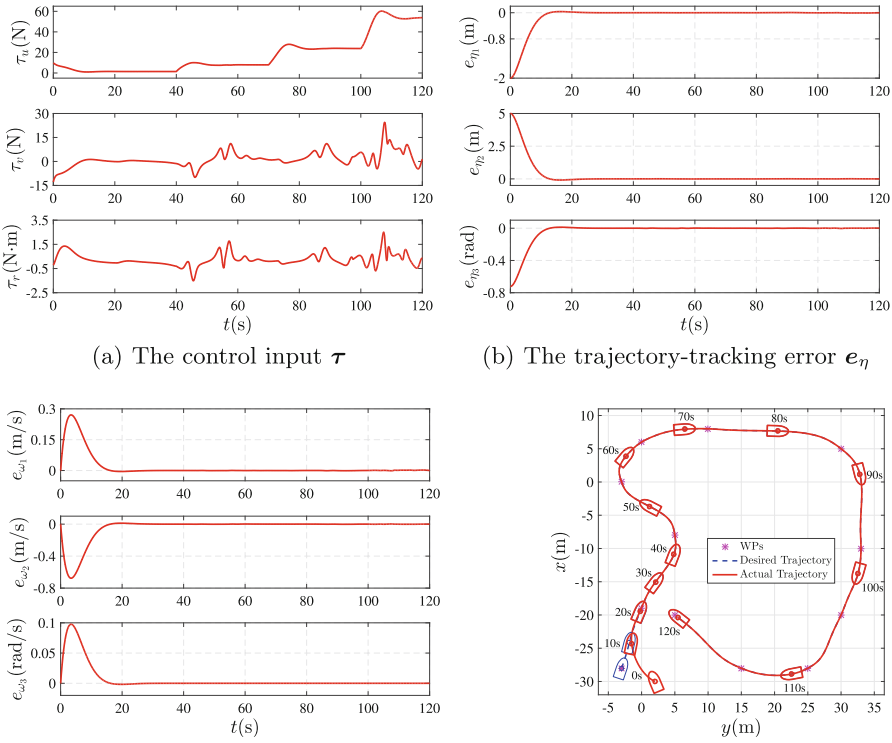

(a) The control input $\boldsymbol{\tau}$ (b) The trajectory-tracking error $\boldsymbol{e}_\eta$

(c) The velocity-tracking error $\boldsymbol{e}_\omega$ (d) The actual trajectory

Fig. 4. The performance of the proposed trajectory-tracking controller.

5 Conclusions

In this paper, a novel TG has been proposed to generate the desired trajectory for the USV in light of successive WPs and reference speed, rather than the trigonometric function or virtual ship method. To be specific, the seventh-order polynominal has been exclusively deployed such that the resultant parameterized path satisfies spatial constraints, and is sufficiently differentiable. Also, the second-order low-pass filter has been exploited to smooth the reference speed, guaranteeing that the generated trajectory and its derivatives are continuous in time. By designing the path speed to meet temporal constraints, the parameterized path has been naturally translated into the time-varying trajectory, which is more practical for users to assign the trajectory-tracking task in advance. Based on the USV model information, the trajectory-tracking controller has been synthesized by virtue of Lyapunov theorem. Eventually, comprehensive simulations conducted on the CyberShip II have verified the effectiveness of both the proposed TG and trajectory-tracking controller. In future work, unmodeled dynamics and external disturbances will be taken into account in the trajectory-tracking control of the USV.

References

1. Fossen, T.I.: Handbook of Marine Craft Hydrodynamics and Motion Control. Wiley, Hoboken (2011)
2. Gao, Y., Wang, N., Zhang, W.: Disturbance observer based finite-time trajectory tracking control of unmanned surface vehicles with unknown dead-zones. In: Youth Academic Annual Conference on Chinese Association Automation, pp. 263–268. IEEE, Hefei, China, May 2017
3. He, H., Wang, N.: Monocular visual servo of unmanned surface vehicles with view-field constraints. In: Chinese Control Decision Conference, pp. 973–978. IEEE, Kunming, China, May 2021
4. Huang, H., Gong, M., Zhuang, Y., Sharma, S., Xu, D.: A new guidance law for trajectory tracking of an underactuated unmanned surface vehicle with parameter perturbations. Ocean Eng. **175**(1), 217–222 (2019)
5. Li, L., Dong, K., Guo, G.: Trajectory tracking control of underactuated surface vessel with full state constraints. Asian J. Control **23**(4), 1762–1771 (2021)
6. Qin, H., Li, C., Sun, Y., Li, X., Du, Y., Deng, Z.: Finite-time trajectory tracking control of unmanned surface vessel with error constraints and input saturations. J. Franklin Inst. **357**(16), 11472–11495 (2020)
7. Qin, H., Li, C., Sun, Y.: Adaptive neural network-based fault-tolerant trajectory-tracking control of unmanned surface vessels with input saturation and error constraints. IET Intel. Transport Syst. **14**(5), 356–363 (2020)
8. Qu, Y., Xiao, B., Fu, Z., Yuan, D.: Trajectory exponential tracking control of unmanned surface ships with external disturbance and system uncertainties. ISA Trans. **78**, 47–55 (2018)
9. Skjetne, R., Fossen, T.I., Kokotović, P.V.: Adaptive maneuvering, with experiments, for a model ship in a marine control laboratory. Automatica **41**(2), 289–298 (2005)
10. Song, S., Park, J.H., Zhang, B., Song, X.: Event-triggered adaptive practical fixed-time trajectory tracking control for unmanned surface vehicle. IEEE Trans. Circuits Syst. II: Express Briefs **68**(1), 436–440 (2021)
11. Stateczny, A., Burdziakowski, P., Najdecka, K., Domagalska-Stateczna, B.: Accuracy of trajectory tracking based on nonlinear guidance logic for hydrographic unmanned surface vessels. Sensors **20**(3), 1–16 (2020)
12. Wang, N., Gao, Y., Zhao, H., Ahn, C.K.: Reinforcement learning-based optimal tracking control of an unknown unmanned surface vehicle. IEEE Trans. Neural Netw. Learn. Syst. **32**(7), 3034–3045 (2021)
13. Wang, N., Ahn, C.K.: Coordinated trajectory tracking control of a marine aerial-surface heterogeneous system. IEEE/ASME Trans. Mechatron. **26**(6), 3198–3210 (2021)
14. Wang, N., Er, M.J., Sun, J.C., Liu, Y.C.: Adaptive robust online constructive fuzzy control of a complex surface vehicle system. IEEE Trans. Cybern. **46**(7), 1511–1523 (2016)
15. Wang, N., Gao, Y., Zhang, X.: Data-driven performance-prescribed reinforcement learning control of an unmanned surface vehicle. IEEE Trans. Neural Netw. Learn. Syst. **32**(12), 5456–5467 (2021)
16. Wang, N., He, H.: Adaptive homography-based visual servo for micro unmanned surface vehicles. Int. J. Adv. Manuf. Technol. **105**(12), 4875–4882 (2019)
17. Wang, N., He, H.: Dynamics-level finite-time fuzzy monocular visual servo of an unmanned surface vehicle. IEEE Trans. Ind. Electron. **67**(11), 9648–9658 (2020)

18. Wang, N., He, H.: Extreme learning-based monocular visual servo of an unmanned surface vessel. IEEE Trans. Ind. Inform. **17**(8), 5152–5163 (2021)
19. Wang, N., Karimi, H.R., Li, H.Y., Su, S.F.: Accurate trajectory tracking of disturbed surface vehicles: a finite-time control approach. IEEE/ASME Trans. Mechatron. **24**(3), 1064–1074 (2019)
20. Wang, N., Su, S.F., Pan, X.X., Yu, X., Xie, G.M.: Yaw-guided trajectory tracking control of an asymmetric underactuated surface vehicle. IEEE Trans. Ind. Inform. **15**(6), 3502–3513 (2019)
21. Wang, N., Zhang, Y., Ahn, C.K., Xu, Q.: Autonomous pilot of unmanned surface vehicles: bridging path planning and tracking. IEEE Trans. Veh. Technol. **71**(3), 2358–2374 (2022)
22. Wang, R., Xue, H., Li, Z., Li, H.W.N., Zhao, H.: Fixed-time trajectory tracking control of an unmanned surface vehicle. In: International Conference on Systems, Science and Engineering, pp. 1–6. Kagawa, Japan, September 2020
23. Xu, D., Liu, Z., Zhou, X., Yang, L., Huang, L.: Trajectory tracking of underactuated unmanned surface vessels: non-singular terminal sliding control with nonlinear disturbance observer. Appl. Sci. **12**(6), 1–17 (2022)
24. Yao, Q.: Fixed-time trajectory tracking control for unmanned surface vessels in the presence of model uncertainties and external disturbances. Int. J. Control **95**(5), 1133–1143 (2022)
25. Zheng, Z., Huang, Y., Xie, L., Zhu, B.: Adaptive trajectory tracking control of a fully actuated surface vessel with asymmetrically constrained input and output. IEEE Trans. Control Syst. Technol. **26**(5), 1851–1859 (2017)